Solar Physics (2023) 298:64
https://doi.org/10.1007/s11207-023-02157-y

RESEARCH

The Possible Cause of Most Intense Geomagnetic Superstorm of the 21st Century on 20 November 2003

Anil Raghav[1] · Zubair Shaikh[2] · P. Vemareddy[3] · Ankush Bhaskar[4] · Omkar Dhamane[1] · Kalpesh Ghag[1] · Prathmesh Tari[1] · Baiju Dayanandan[5] · Badar Mohammed Al Suti[5]

Received: 30 January 2023 / Accepted: 14 April 2023 / Published online: 17 May 2023

Abstract

An extreme geomagnetic storm has the potential to affect various technologies and activities in space and on the ground, e.g., power grids, oil and gas industries, communications, ground transportation, satellite infrastructure, global navigation satellite systems, aviation, etc. Therefore, it is considered a major source of risk by various governmental agencies and corporations at the international level. All notable space weather events (superstorms) are caused by interplanetary coronal mass ejections (ICMEs). But not every ICME leads to an extreme storm. Moreover, how does an extreme storm form? Or which explicit characteristic of ICME actually is responsible for inducing a superstorm? Here, we re-investigate the ICME characteristics that contribute to the most intense storm of the current century that occurred on 20 November 2003. Interestingly, the studied ICME magnetic cloud shows characteristics of extremely flattened (pancaked) structure i.e. quasi-planar magnetic structure (PMS). The pancaked ICME shows less adiabatic expansion than usual in the compressed direction, which leads to strong magnetic field strength, high plasma density, high solar wind speed, high dynamic pressure, and a high eastward interplanetary electric field. Here, we propose that the ICME that transformed into a quasi-PMS has the aforementioned enhanced features with strong southward magnetic field component that contributes to efficiently transferring plasma and energy into the Earth's magnetosphere to cause the observed superstorm.

Keywords The Sun: coronal mass ejections (CMEs) · Solar-terrestrial relations · Heliosphere · Solar wind

✉ A. Raghav
anil.raghav@physics.mu.ac.in

1 Department of Physics, University of Mumbai, Vidyanagari, Santacruz (E), Mumbai 400098, India

2 Indian Institute of Geomagnetism (IIG), Kalamboli, New Panvel, Navi Mumbai 410218, India

3 Indian Institute of Astrophysics, II Block, Koramangala, Bengaluru 560034, India

4 Vikram Sarabhai Space Centre (VSSC), Indian Space Research Organisation (ISRO), Thiruvananthapuram, Kerala 695022, India

5 Department of Mathematical and Physical Sciences, College of Arts and Science, University of Nizwa, Nizwa, Oman

1. Introduction

Historically, the largest on record extreme geomagnetic superstorm occurred in September 1859 known as the 'Carrington' event (Cannon et al., 2013; Schrijver and Siscoe, 2010). It was nearly three times stronger than the largest superstorm of the space age that happened in March 1989 (Lakhina et al., 2005; Cliver and Svalgaard, 2004), which caused the well-known failure of the Quebec power grid and damaged two transformers in the United Kingdom (Cliver and Svalgaard, 2004). This led to a power blackout for 9 hours, affecting 5 million people in cold weather of Canada, and caused an overall business loss of USD 2 billion approximately (Hapgood, 2012). In fact, many of the space agencies lost track of some 1600 spacecraft temporally (Hapgood, 2012). The most recent superstorm took place in October–November 2003, which caused a 90 min blackout and affected 50,000 people in Sweden (Eastwood et al., 2017). Also, historical magnetogram records show many intense storm occurrences in the past (Hayakawa et al., 2020). If such an intense storm were to occur today, it would pose a high threat to spacecraft and ground infrastructure. (Oliveira et al., 2020). Geomagnetic superstorms, therefore, present a serious threat to our technology-dependent modern society, and studying what causes these events is therefore highly essential (Liu et al., 2014; Eastwood et al., 2017).

In general, the southward component of the interplanetary magnetic field (IMF) and the eastward interplanetary electric field are the fundamental cause of geomagnetic storm (Daglis et al., 1999; Gonzalez and Tsurutani, 1987; Gonzalez et al., 1994; Tsurutani et al., 1988; Akasofu, 2018). The day-side and night-side magnetic re-connection allows the energy and plasma transfer between solar wind and Earth's magnetosphere (Dungey, 1961; Gonzalez and Mozer, 1974; Akasofu, 1981). The large scale magnetic structures in the solar wind such as interplanetary coronal mass ejections (ICMEs) or corotating interaction regions (CIRs) are the main interplanetary agents which cause geomagnetic storms (Tsurutani and Gonzalez, 1997). The reported studies suggest that CIRs generally trigger weak or moderate storms (Chi et al., 2018; Tsurutani et al., 2006), whereas ICMEs contribute to intense or severe storms, sometimes superstorms (Gonzalez et al., 1989; Tsurutani et al., 1988; Echer et al., 2008; Zhang et al., 2007; Tsurutani et al., 1992). However, the link between ICME features and the intensity of the storm is poorly understood. Thus, forecasting of a superstorm or severe storm is difficult to date when ICME hits the Earth's magnetosphere.

Planar magnetic structures (PMS) are frequently seen in corotating interaction regions (CIRs) and sheath regions caused by interplanetary coronal mass ejections (ICMEs). PMS refers to large-scale, sheet-like magnetic fields embedded within the ICME structure. These structures can be formed through the process of magnetic reconnection, which can occur as the ICME/CIR propagates through the solar wind. Recently Shaikh et al. (2020) and Shaikh and Raghav (2022) statistically examined the plasma properties within planar and non-planar ICME sheath regions and magnetic cloud (MC) regions using in situ data from the Advanced Composition Explore (ACE) satellite. Their study found that planar sheaths and quasi-planar MC had greater average plasma temperature, density, speed, plasma beta, thermal pressure, and magnetic pressure than non-planar sheaths. Their analysis demonstrates that strong compression is critical in the formation of PMS in sheath regions or MC regions. Interestingly, their analysis shows that the intensity of the southward/northward magnetic field component is about twice as strong in planar sheath regions and MC regions as it is in non-planar regions. Therefore, compared to non-planar ICMEs, planar ICME sheaths, and MCs are expected to have enhanced geo-effectiveness. So, in this article, we look into a case study of a planar ICME and its impact on the geomagnetic storm.

The time series of the Dst index (used to quantify the intensity of the storm) indicates that the largest storm of the current century occurred on 20 November 2003 (Gopalswamy et al.,

2005b). Kumar et al. (2011) study this event and suggest that the interaction of two CMEs produced southward IMF for a long time. Moreover, Grechnev et al. (2014b) suggest that ICME MC has narrow-angle $\leq 14^{\circ}$ with a spheromak configuration, which shows a very strong magnetic field ~ 56 nT with the unusual weak expansion caused by the preceding ICMEs. In addition, Kataoka et al. (2005b) present evidence for the density effect during the main phase of the superstorm. The density controls the Mach number and hence the compression ratio, which controls energy transfer and the transpolar potential from solar wind to magnetosphere (Akasofu, 1981). Besides, Fok et al. (2011) proposed that O^{+} is the dominant species over H^{+} in the ring current during the main to the mid-recovery phase of the storm. Grechnev et al. (2014a) suggest that source of this superstorm is a possible additional eruption above the bifurcation region close to the solar disk center. Srivastava et al. (2009) suggest that a flare associated with the CME, occurred at a location marked by high magnetic field gradient, led to the release of free energy stored in the active region, which could be the reason for this superstorm. During this superstorm, various activities and effects have been observed in the magnetosphere (Balasis et al., 2012), plasma-sphere (Chi et al., 2005), ionosphere (Mannucci et al., 2005) and thermosphere (Bruinsma et al., 2006) of the Earth. Interestingly, during the Halloween storm of 2003, the Van Allen belt was compressed dramatically such that the outer belt had its center only 10,000 km from Earth's equatorial surface, and similarly, it was also observed during the studied storm (Baker et al., 2004). Shprits et al. (2006) proposed the formation of a new radiation belt during the 2003 Halloween storm. The corresponding ICME is, therefore, a causal agent of various observed technological effects and severe space weather conditions. This study presents the case study of the most intense geomagnetic storm of the 21st century on 20 November 2003. To unravel the distinct characteristic of this ICME, we investigate 5 min time resolution data from the OMNI database.

2. Observation

The temporal evolution of the in situ interplanetary plasma parameters and magnetic field are shown in Figure 1. The different colors are used to represent important interplanetary sub-structures, i.e., sheath and magnetic cloud (see Figure 1). The commencement of the ICME shock-front is recognized with sudden sharp enhancement in IMF (B_{mag}), solar wind speed (V_p), Plasma dynamic pressure (P_{dyn}), convection electric field (E), proton temperature (T_p), and proton density (N_p) (see the first vertical black dash line). The ICME sheath region is identified with high N_p, T_p, V_p, and plasma beta (β); large fluctuations in IMF vectors (i.e., $B_{x,y,z}$) (Shaikh, Raghav, and Bhaskar, 2017; Kilpua, Koskinen, and Pulkkinen, 2017; Raghav et al., 2014; Raghav and Kule, 2018b). The sheath is followed by lower fluctuations in B_{mag} and B_{comp}, slow rotation in θ and ϕ, the gradual decrease in V_p, low β & T_p, indicate the transit of magnetic cloud (Zurbuchen and Richardson, 2006; Raghav and Kule, 2018a,b). The detailed information about the ICME shock at the bow shock nose of the Earth and at L1 point is available at http://ipshocks.fi/database. The database suggests that it is quasi-perpendicular fast forward (FF) shock with the shock normal $\hat{n} = (-0.93, 0.10, -0.35)$, shock speed $V_{sh} = 673$ km s^{-1}, magneto-sonic Mach number $M_{ms} = 3.2$, and the angle between shock normal and magnetic field $\theta_{Bn} = 68.0^{\circ}$ at the Earth's bow shock.

2.1. Source Region Analysis

The active region NOAA 10501 is identified to be the source region of the CME observed on 18 November 2003. The source region was located near the disk center (N03E08) so that

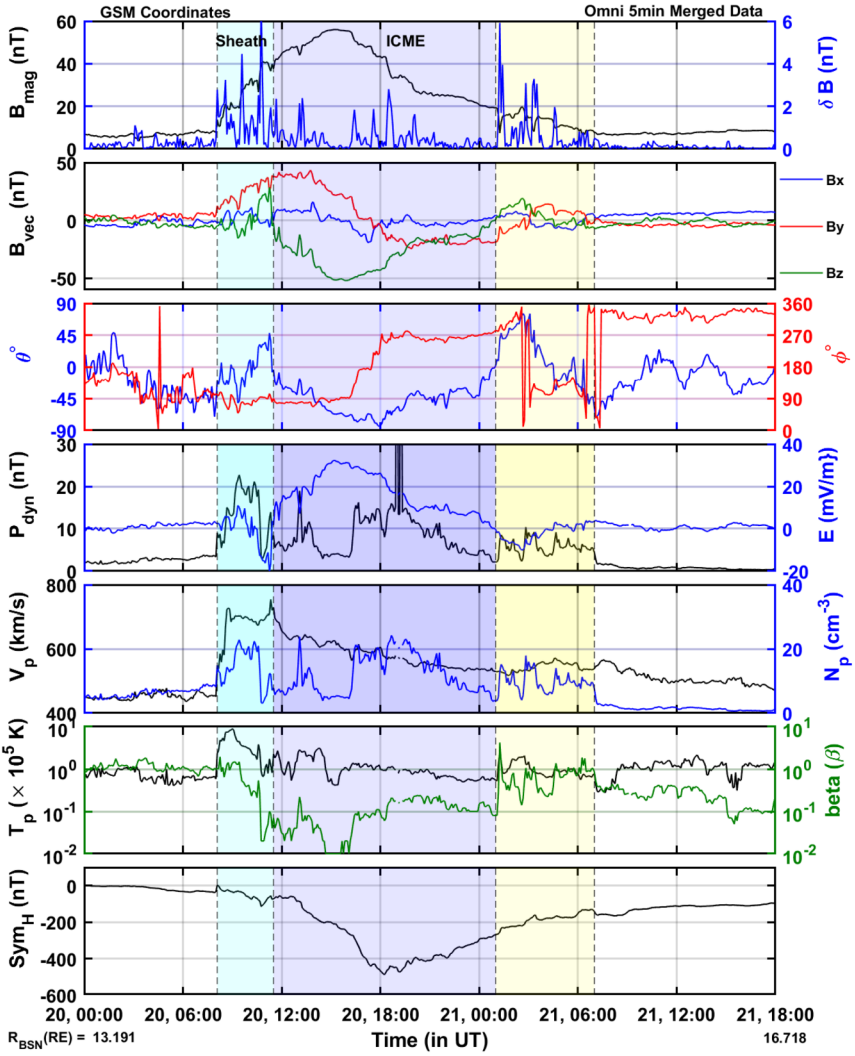

Figure 1 An ICME crosses the Earth's bow shock on 20 November 2003. The top to bottom panels represent different interplanetary parameters such as: total interplanetary field strength IMF B_{mag} and absolute value of IMF fluctuation δB, IMF vectors, i.e., B_{vec}, azimuth ϕ° and elevation θ° angle, Plasma dynamic pressure (P_{dyn}) and plasma convective electric field E, solar wind speed V_p and proton density (N_p), Temperature (T_p) and plasma beta (β), and geomagnetic storm index (Sym_H) respectively. The shaded regions represent the ICME shock-sheath (cyan), magnetic cloud (purple), and trailing solar wind region (yellow). The observations are in GSM coordinate system.

the CME impacts the Sun–Earth line. Subsequently, the CME caused the strongest magnetic storm of the Solar Cycle 23 as observed by the in situ instruments. From Figure 2a, the MLSO Hα images show a semi-circular filament above the polarity inversion line of the magnetic field in the south part of the AR. Filaments are considered precursor features of CMEs, and often, CME eruption follows the filament disappearance. From these Hα images, the filament erupted at 07:53 UT followed by an M3.9 class flare as observed in GOES X-ray light curve. The start time of the flare is 08:12 UT, and the peak time is 08:30 UT. A detailed

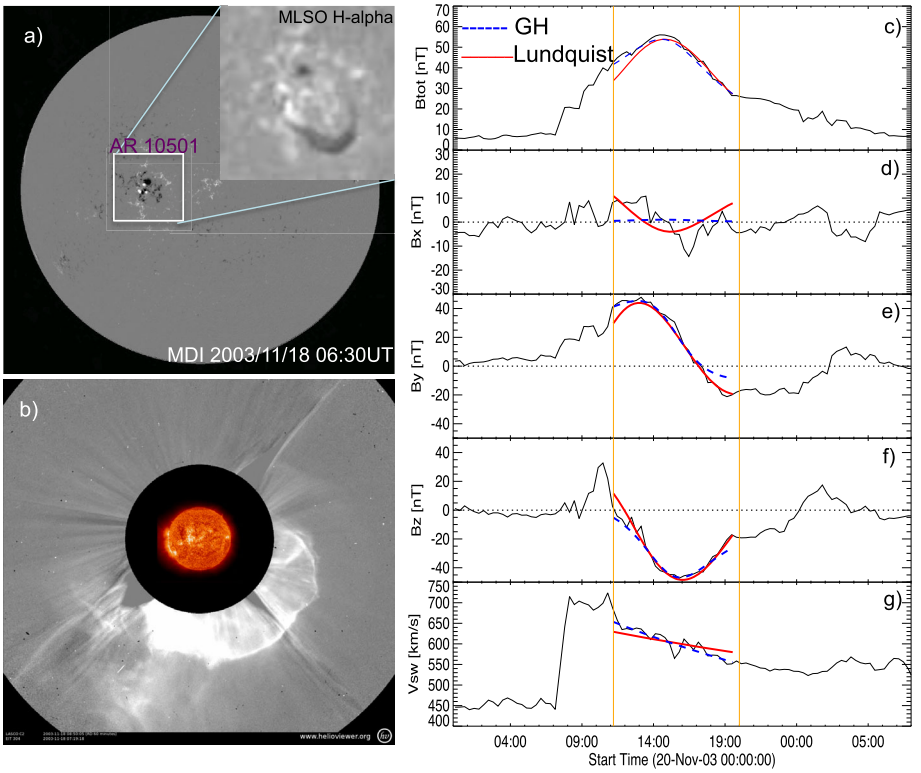

Figure 2 Observations illustrating the Sun–Earth connection of the 18 November 2003 CME event. a) MDI magnetogram showing the source AR 10501. Inset is the Hα image of the AR presenting a dark filament, b) LASCO/C2 white light observation showing the launch of the associated CME from the source AR 11501. Image of the Sun from SOHO/EIT 304 Å is displayed within the occulting disk, (c-g) In situ observations of the CME as magnetic cloud viz., magnetic field strength ($B_{\rm tot}$) and its components (B_x, B_y, B_z), and solar wind speed ($V_{\rm sw}$). Within the flux rope interval (vertical orange lines), the blue dashed and solid red curves represent the fitting results by the Gold-Hoyle and Lundquist models, respectively.

study by Chandra et al. (2010) inferred that the filament channel exhibits dextral barbs in some parts and sinistral barbs in other parts. Although the total helicity injection from the AR was negative, the erupting part of the filament section was reported to be injected with the positive sign of helicity, and, therefore, the MC was expected to have positive helicity.

With this on disk observation of the filament eruption, a CME was recorded in LASCO white light coronagraphs on 18 November at 08:50 UT. From the morphology of Figure 2b, the CME appeared to be oriented in south-west direction. The average linear speed of this CME was measured as 1660 km s^{-1} in LASCO field-of-view. When this CME arrived at the Earth on 20 November the strongest geomagnetic storm (Dst 472 nT, see Figure 1) in this century was observed (Gopalswamy et al., 2005a; Srivastava et al., 2009).

2.2. Model Analysis

In Figure 2(c-g), the in situ observations of the magnetic field are fitted with the Lundquist (Lundquist, 1950) and Gold-Hoyle (GH; Gold and Hoyle, 1960) models of cylindrically symmetric linear force-free magnetic fields. The fitting accounts for the expansion of the

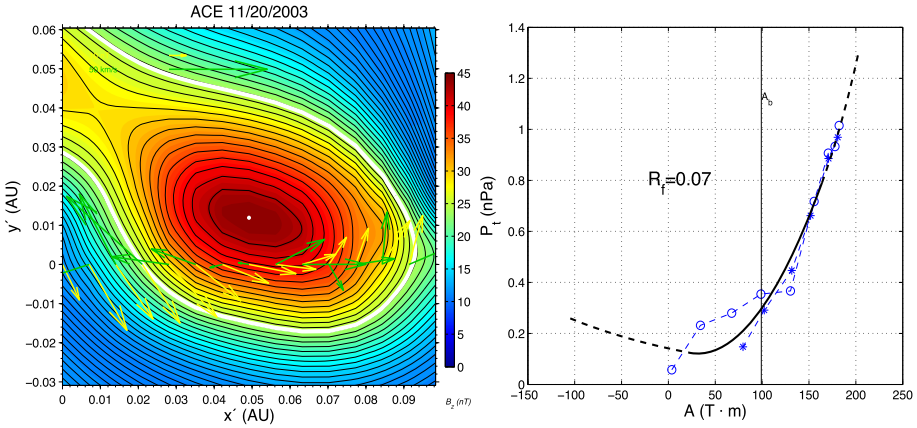

Figure 3 Left: Grad-Shafranov reconstruction of the cross-section of the magnetic cloud observed by the ACE spacecraft. The contours refer to the vector potential (A) with the flux rope boundary indicated with white thick contour. The B_z distribution is color scaled as shown by the color bar. Transverse magnetic (velocity) field vectors are shown with yellow (green) arrows along the $y = 0$ line. The orientation of these arrows implies right-handed chirality of the magnetic field in the flux rope associated with this magnetic cloud. Right: the data plot and fitting curve for $P_t(A)$ of the magnetic cloud event. The data points are spacecraft measurements, circles for the first half of the event, and stars for the second half. The solid curve represents the fitting function, $P_t(A)$.

magnetic cloud (Vemareddy et al., 2016) during the spacecraft passage. Compared to the Lundquist model, the GH fit represents a good model in terms of rms value. From these fits, the MC axis is oriented 55° south in latitude and around 130° in longitude. This means that the MC had a significant southward B_z component of the magnetic field to launch the geomagnetic storm. The flux rope has a positive sign of magnetic helicity consistent with the source region helicity sign of the erupting part of the filament as seen in Hα images. The twist of the magnetic field in the flux rope is 3.9 turns. The MC has a diameter of 0.1 AU and underwent significant expansion at a rate of 0.48 per day.

The flux rope cross section is constructed with Grad-Shafranov (GS) reconstruction technique (Hu and Sonnerup, 2002) which is displayed in Figure 3. The cross section is typically shown with contours of the flux function (A) and filled contour map of B_z. The MC boundary is identified with white thick contour, containing a slightly smaller interval than the MC interval as given by the boundaries in Figure 2. Transverse magnetic field is shown with yellow arrows along $Y = 0$ line and represents helical field lines winding the axis in right-hand (clockwise) direction in projection. The GS reconstruction includes minimum variance analysis of magnetic field vectors and construction of residue maps. From this analysis of the GS reconstruction procedure, the MC axis is found to be oriented at $-47°$ latitude and 133° longitude, which is also consistent with the MC fit procedure described above. A residue value $R_f = 0.07$ quantitatively describes the goodness of fit to the $P_t(A)$.

2.3. PMS Identification

The minimum variance analysis (MVA) technique has been employed to investigate the features of ICME. The MVA analysis gives three eigenvalues (λ_1, λ_2, and λ_3) as output in descending order. There exist three eigenvectors ($\boldsymbol{e_1}$, $\boldsymbol{e_2}$, and $\boldsymbol{e_3}$) corresponding to each eigenvalue. IMF vectors B_1^*, B_2^*, and B_3^* have been estimated via MVA analysis corresponding

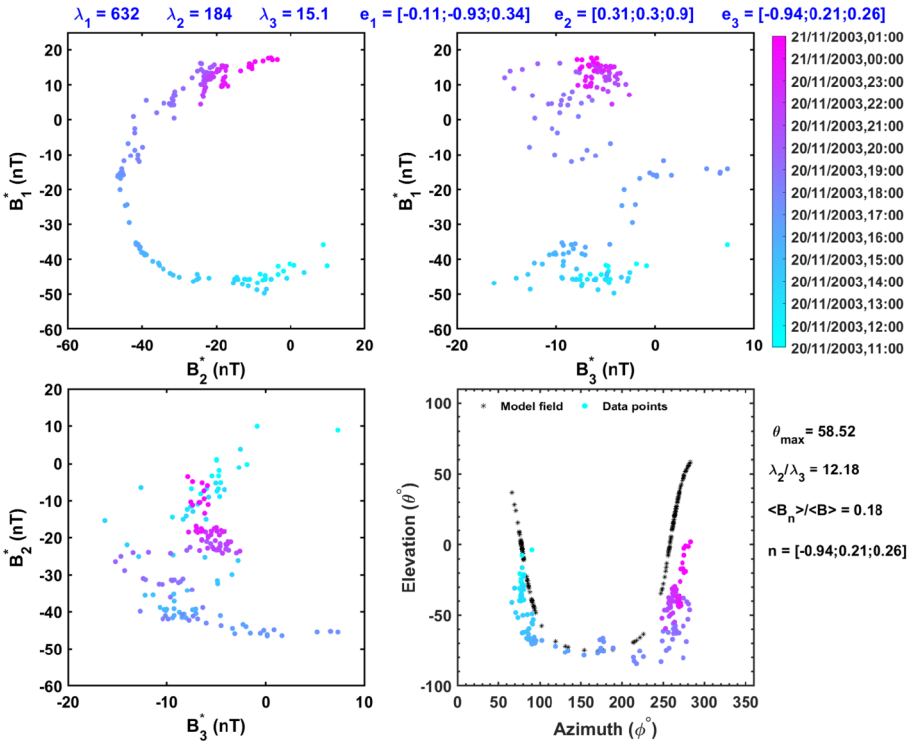

Figure 4 Top two panels and bottom left panel present hodogram plots of the ICME magnetic cloud region in a different plane of projections. B_1*, B_2*, and B_3* (corresponding to maximum (λ_1), intermediate (λ_2), and minimum (λ_3) eigenvalues) are the magnetic field vectors from the MVA analysis. Bottom right panel shows the distribution of azimuth (ϕ) vs. elevation (θ) angle of IMF in GSM co-ordinate system for the ICME magnetic cloud region (as shown in Figure 1). The $\frac{\lambda_2}{\lambda_3}$, $\frac{<B_n>}{B}$, and n give the information about the efficiency, planarity, and normal direction of the PMS, respectively. The θ_{max} is inclination of the PMS plane w.r.t. the ecliptic plane. When IMF vectors $\boldsymbol{B} = (B_x, B_y, B_z) \equiv (Bcos\theta cos\phi, Bcos\theta sin\phi, Bsin\theta)$ are parallel to a plane whose normal is $\boldsymbol{n} \equiv (n_x, n_y, n_z)$, the relation between ϕ and θ is given as (Nakagawa, Nishida, and Saito, 1989; Palmerio, Kilpua, and Savani, 2016): $n_x cos\theta cos\phi + n_y cos\theta sin\phi + n_z sin\theta = 0$. The fitted curve (see the black dotted curve) to the measured (colored dots) ϕ and θ indicates the presence of PMS.

to the maximum, intermediate, and minimum variance directions (Sonnerup and Scheible, 1998). The reported studies used the following criteria to identify PMS in the solar wind (Nakagawa, Nishida, and Saito, 1989; Nakagawa, 1993; Neugebauer, Clay, and Gosling, 1993): (i) a wide distribution of the azimuth (ϕ) angle, i.e., $0° < \phi < 360°$, (ii) good planarity, i.e., $\frac{|B_n|}{B} \leq 0.2$, and (iii) good efficiency $R = \frac{\lambda_2}{\lambda_3} \geq 3$, respectively (Palmerio, Kilpua, and Savani, 2016; Shaikh et al., 2018; Shaikh, Raghav, and Vichare, 2019; Jones and Balogh, 2001). Here, B is the magnitude of IMF, and B_n is component of the magnetic field normal to the PMS plane, i.e., $B_n = \boldsymbol{B} \cdot \boldsymbol{n}$, where, $\hat{n}$ is the normal direction of the PMS plane calculated by the MVA technique (Sonnerup and Scheible, 1998; Lepping and Behannon, 1980). A PMS will have a perfect planarity when $B_n = 0$. This implies that a low value of $\frac{|B_n|}{B}$ is a good indicator that vectors are almost parallel to a plane (Neugebauer, Clay, and Gosling, 1993; Shaikh et al., 2019; Nakagawa, Nishida, and Saito, 1989).

Figure 4 represents hodogram plots in different plane projections (top row and bottom left subplots) and the distribution of the elevation (θ) and azimuth (ϕ) angle of IMF for the

ICME magnetic cloud region (bottom right) shown in Figure 1. The 2D hodogram represents a semicircular shape in the projection of intermediate and maximum planes (see top right pane in Figure 4). It clearly demonstrates the traditional magnetic cloud feature and suggests the smooth rotation of the magnetic field vector that represents an inbuilt feature of the magnetic cloud. It is important to note that Nakagawa, Nishida, and Saito (1989), Nakagawa (1993) suggest differences between MC and PMS based on $\theta - \phi$ diagram while studying PMSs inside the sheath regions. They have never found a wave-like pattern for magnetic cloud (Nakagawa, Nishida, and Saito, 1989; Nakagawa, 1993). However, here the $\theta - \phi$ distribution diagram shows a wave-like pattern, which is a typical signature of the possible existence of PMS. The estimated planarity ($|B_n|/ < B >$) is 0.18, and the efficiency λ_2/λ_3 is 12.18. Therefore, we argue that the MC transformed into a quasi-PMS, and we call them either quasi-planar magnetic clouds or pancaking of magnetic cloud (Nakagawa, Nishida, and Saito, 1989; Neugebauer, Clay, and Gosling, 1993; Jones, Balogh, and Horbury, 1999; Raghav and Shaikh, 2020). Also note that in PMSs, the magnetic field vector is confined to a particular plane, and that plane can rotate in any direction. The plane of quasi-planar magnetic cloud analyzed here is inclined with respect to the ecliptic plane with $\theta_{max} = 58.52^{\circ}$ and the normal direction of the plane is $\boldsymbol{n} = (-0.94, 0.21, 0.26)$. Moreover, at $\theta = 0$, the plane intersects at $\sim \phi = 77.67^{\circ}$ and 258.00°, this indicates that PMS plane includes the Archimedean spiral direction (Nakagawa, 1993; Jones, Balogh, and Horbury, 1999; Kilpua, Koskinen, and Pulkkinen, 2017).

3. Analysis and Discussion

In general, the MVA technique is routinely used to study PMSs (Nakagawa, 1993; Kataoka et al., 2005a; Shaikh et al., 2018) and ICME magnetic clouds (Burlaga et al., 1981). The criteria listed for PMSs may apply for magnetic clouds crossed at a low impact parameter. In that case, the eigenvalues are well separated, the B_n component is low, and there is a clear rotation of the azimuthal angle. The MC axis is considered to be the intermediate eigenvector. In that view, the MC is a quasi-2D structure with an invariance along the direction of the intermediate eigenvector, and the magnetic field rotates in the plane of the MC cross section. Burlaga et al. (1981) suggested that the magnetic field configuration is substantially planar and highly organized on a large scale. However, in general, PMSs demonstrate a characteristic feature when the interplanetary magnetic field vectors are plotted in a $\phi - \theta$ space. It implies that the field vectors in PMSs are not scattered randomly but distributed over the full range of ϕ and depict a distinct curve in the $\phi - \theta$ (Nakagawa, 1993). In addition, Nakagawa, Nishida, and Saito (1989), Nakagawa (1993) suggested that a non-planar magnetic cloud can demonstrate confinement of magnetic field vectors to a plane but does not show wide distribution, i.e., wave-like configuration.

The various reported studies suggest stretching and flattening of the shape as ICME propagates radially away from the Sun (Riley and Crooker, 2004; Owens, Merkin, and Riley, 2006; Savani et al., 2011; Davies et al., 2021). The relation between expansion velocity and the aspect ratio of ICME has been utilized to interpret the deformation of the flux rope. In general, an ICME expands in all directions whereas the solar wind expands only in the non-radial directions. Thus, the plasma pressure in an ICME decreases rapidly compared to the solar wind. This leads to the decrease in the expansion velocity of ICME and further to an increase in the aspect ratio. The complete process implies that the lower internal pressure reduces the strength of the ICME expansion resulting in flattening the cross section. (Savani

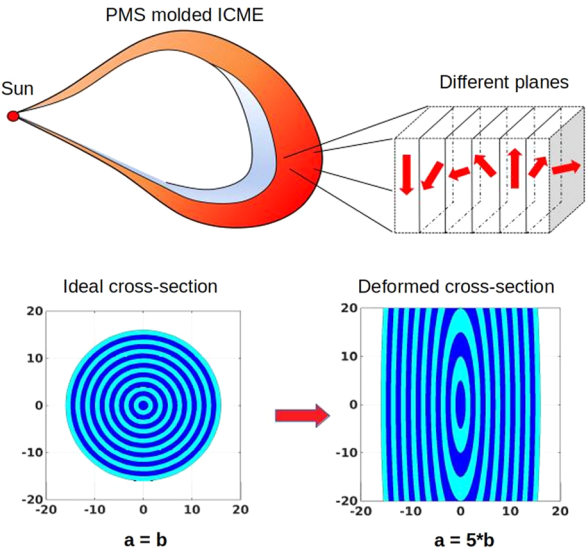

Figure 5 Schematic presentation of PMS molded ICME, and the visualization of an ideal and deformed cross section of a magnetic cloud.

et al., 2011). Moreover, the numerical simulations have been employed to study the propagation of ICMEs to connect the evolutionary changes and the CME morphology (Riley, Linker, and Mikić, 2001; Odstrcil, Riley, and Zhao, 2004; Manchester et al., 2004; Kataoka et al., 2009; Nakamizo et al., 2009; Shiota et al., 2010; Feng, 2020). They suggested that ICME evolved into flattened objects along with its evolution and referred to as 'pancaked ICME' (Riley and Crooker, 2004; Savani et al., 2011).

The studied ICME is followed by another ICME, which shows the hump in solar wind speed, enhancement in plasma beta, temperature, density, dynamic pressure, high fluctuations in the total magnetic field, and smooth rotation in IMF components as well as in its elevation angle (see Figure 1 yellow shaded region). However, the high dynamic pressure of the trailing region sets up the compression in the studied ICME along the direction of the solar wind flow. Thus, the concentric surface layers of the hypothetical circular cross section of the ICME cramp closer to each other. But, no compression exists along the y- or z-direction, and expansion of the magnetic cloud is possible in these directions as usual. This anisotropic expansion may lead to the distortion of the initially circular cross section into an elliptical shape with a minor axis (along the compression, i.e., usually x-axis) and the major axis along the z-axis (assuming that the y-axis represents the axis of the flux rope). This is also corroborated by the GS reconstruction analysis that demonstrates a nearly elliptical cross section of flux rope (see Figure 3). Note that the employed GS reconstruction estimation assumed cylindrical flux-rope structure. Thus, the reconstruction cross section based on deformed (elliptical-cylindrical) flux-rope structures may provide evidences of highly flattened flux rope cross section. Moreover, the wide range wave-like distribution of ϕ in $\phi - \theta$ diagram confirms the quasi-planar modulation of magnetic cloud.

Numerous studies have identified the importance of CME-CME interactions (Zhang et al., 2007; Desai et al., 2020; Lugaz et al., 2017; Liu et al., 2014; Wu et al., 2022). More specifically, Koehn et al. (2022) studied the CME-CME interaction using numerical simulations and quantified the CME compression and its geo-effectiveness. In their simulation, they varied the launch time of two CMEs and demonstrated different interaction conditions and simulated their response at 1 AU. The various mergers produced diverse geophysical

impacts with different solar wind variables. The prolonged interaction can maximize dynamic pressures due to the merger of the CME sheath regions. Therefore, we think that ICME pancaking might result from CME-CME or CME-CIR interactions. The magnetic field and plasma properties can be altered due to such interaction. We observed enhancement in IMF field magnitude and the smooth rotation of the magnetic field components after the trailing edge of the pancaked ICME (see Figure IP). We found a low proton number density but enhanced in plasma beta for the same region. Thus, we conclude that the studied pancaked ICME is followed by another ICME-like flux-rope structure. Therefore, we assume that the CME-CME interaction leads to the compression of the studied ICME, which further transforms into a quasi-planar structure.

There are several physical processes responsible for the generation of an intense or great geomagnetic storm. Tsurutani et al. (1988) concluded that IMF B_z plays a primary role compared to the solar wind speed for major storms. Gonzalez et al. (1998) found that the peak magnetic-field strength and the peak velocity values associated with ICME magnetic cloud contribute to great geophysical consequences. Reported studies demonstrate that the time-integrated electric field E_y is a key parameter in the severity of magnetic storms (Echer et al., 2008; Kumar et al., 2015; Balan et al., 2014). Zhang et al. (2006) pointed out the contribution of plasma density and dynamic pressure in intense and moderate storms.

Figure 6(a) shows the observed Dst index, pressure corrected Dst (Dst*) and modeled Dst index for the event. Dst* is estimated according to O'Brien and McPherron (2002). Dst* is nothing but the corrected Dst for solar wind pressure-induced currents other than ring current. Clearly, the peak amplitude of Dst has become larger (i.e., Dst*), implying the role of solar wind pressure influence. Further, we compare observed Dst index with model estimates using the Temerin and Li (2002) model, which is explicitly based on solar wind parameters. This empirical model reproduces an overall profile of the observed Dst, while the peak amplitude of Dst is not well reproduced for this storm even though the model is known to have good efficiency. This mismatch in amplitude could be due to some physical processes not very well accounted for the model. PMS structure and piling effect could be one of those.

The solar wind data indicates the elevated pressure during and after the transit of ICME. This has significant importance as the magnetosphere is highly compressed during this. The quantitative estimates of this compression could be represented by empirical magnetopause models such as Shue et al. (1998). The bottom panel of Figure 6 shows the standoff magnetopause distance estimated using the empirical model by Shue et al. (1998). The time series shows the magnetosphere was highly compressed during the storm, the magnetopause moved as close to as 6 Re.

We agree the magnetopause stand-off distance is extremely low. This is possibly due to the very high B_z (~ -50 nT) along with the high dynamic pressure value during the storm, which has caused the erosion of the day-side magnetosphere. However, note that the model used in this study is empirical in nature, and such extreme compression has not been confirmed by in situ measurements. So, the values it predicts are based on solar wind data and may not be real. Moreover, there are simulation studies that have reported the possibility of such extreme compression of the magnetosphere [e.g., Ngwira et al. (2013), Welling et al. (2021)]. Welling et al. (2021) showed for the northward IMF case, the stand-off distance is ~ 4.41 R_e; whereas, for the southward case, day-side re-connection further erodes the magnetopause to a stand-off distance of 2.84 R_e.

The studied event is the largest geomagnetic storm of the current century with a Dst index of -472 nT. The associated ICME magnetic cloud had high inclination to the ecliptic plane,

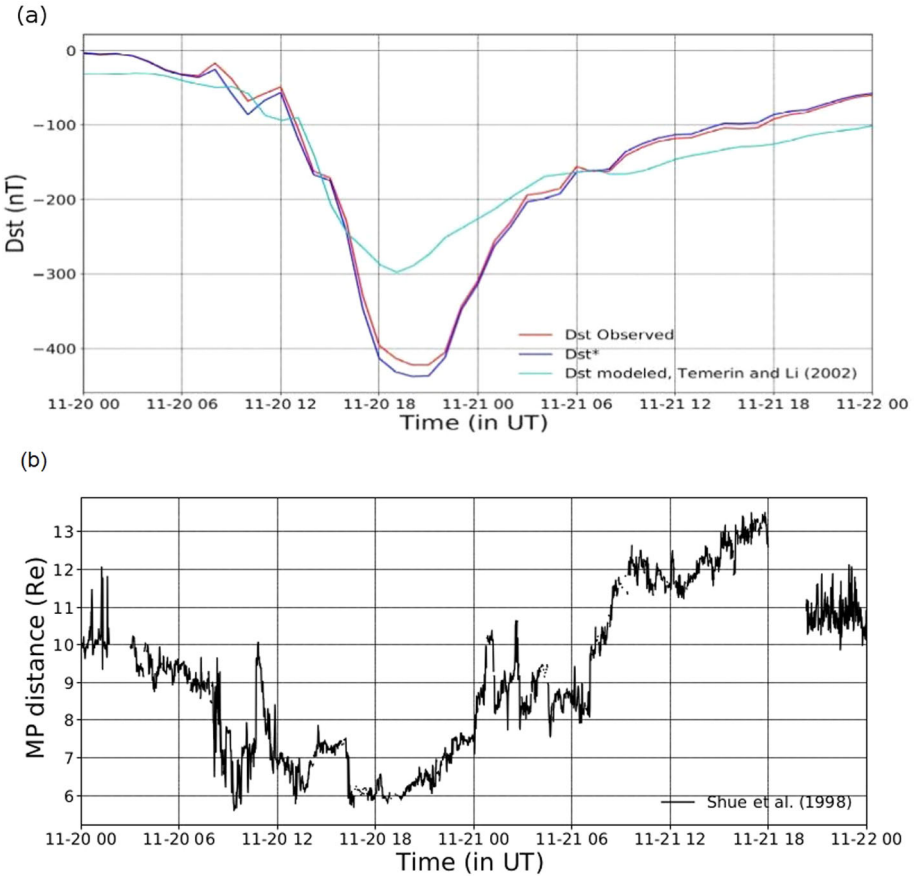

Figure 6 (a) Temporal variation of observed Dst index, pressure corrected Dst (Dst*) (O'Brien and McPherron, 2002) and Temerin and Li (2002) model output during the selected storm. (b) The temporal variation of estimated standoff magnetopause distance using Shue et al. (1998).

high magnetic field ~ 56 nT, $B_z = \sim -50$ nT, and arrived with speed of ~ 730 km s^{-1} (Gopalswamy et al., 2005b). Furthermore, a high number density, temperature, dynamic pressure, and convective electric field (see Figure 1) are observed during the ICME magnetic cloud transit. The enhanced plasma parameter values could be associated with compression of the magnetic cloud. It is further supported by the enhanced plasma β value in the trailing part of the cloud.

The studies reported in the literature found PMS inside the ICME shock-sheath. Their evolution in the sheath is caused either by the process that (i) aligned magnetic field lines of the solar wind parallel to the surface magnetic cloud and draped the plasma around them or by (ii) the high compression aligned the pre-existing micro-structures and discontinuities parallel to the shock plane in the downstream region of solar wind (Nakagawa, 1993; Neugebauer, Clay, and Gosling, 1993; Farrugia et al., 1990; Kilpua, Koskinen, and Pulkkinen, 2017; Shaikh et al., 2019, 2018). In addition, Kataoka et al. (2015) proposed 'pileup accident' hypothesis to explain the extreme storm on 17 March 2015 induced by ICME sheath molded PMS.

Recently, Raghav and Shaikh (2020) provided the first verification of PMS molded ICME (could be similar to pancaking) using Wind spacecraft data. They assumed the higher aspect ratios are possible for ICMEs at 1 AU and demonstrated their effect on the cross section. They suggested that a passage of a spacecraft through a highly flattened cross section of the flux rope may interpreted as quasi-2D planar magnetic structure. Moreover, it is also implied that the rotation of the magnetic field vector remains the intact feature of MC, and one should observe semi-elliptical shape in the hodogram plot. The schematic demonstration of the PMS molded ICME and deformed cross section is shown in Figure 5. Thus, we conclude that the high compression from the leading or trailing end of ICME produces a compact magnetic cloud that further transforms into the quasi-2D structure like PMS. In addition, we have recently analyzed 468 ICME events in which about 35% of sheath events indicate planarity signature, and 29% of MC events suggest quasi-planar evidence (Shaikh et al., 2020; Shaikh and Raghav, 2022).

Here, we suggest that the ICME to PMS transformation process leads to a weaker adiabatic expansion of the magnetic cloud than expected, keeping high speed, high density and strong magnetic field within the magnetic cloud (in particular, enhanced B_z component of IMF), high dynamic pressure and integrated electric field. All these plasma parameters individually drive the intense or moderate geomagnetic storm. Thus, we conclude that the rarest combination of all the enhanced plasma parameters associated with pancaked (highly flattened) ICME drives the largest superstorm of the current century and compression of plasmasphere and radiation belt. The CME-CME or CME-CIR interaction may induce such pancaking of the ICME magnetic cloud, further leading to intense or extreme storms (Liu et al., 2014; Koehn et al., 2022). Also, note that the pancaked ICME will affect its arrival time prediction at the Earth. A detailed investigation is needed in this direction.

4. Conclusion

Here, we focus on the investigation of extreme storms and examine the case study of the most intense geomagnetic storm of the 21st century on 20 November 2003. In conclusion:

- The studied event is the most intense geomagnetic storm of the current century with a Dst index of -472 nT.
- The CME-CME interaction leads to the compression of the studied ICME, which further transforms into a quasi-planar structure.
- We conclude that the ICME to PMS transformation process results in a weaker adiabatic expansion of the magnetic cloud than anticipated, maintaining the magnetic cloud's high speed, high density, and strong magnetic field (significantly enhanced B_z component of IMF), high dynamic pressure, and electric field.
- The combination of all the enhanced plasma parameters and IMF strength associated with pancaked (highly flattened) ICME drive the most intense superstorm of the current century.
- The time series variation of standoff magnetopause distance estimated using the empirical model by Shue et al. (1998) shows the magnetosphere was highly compressed during the storm. The magnetopause boundary moved as close to 6 R_e implies the compression of the plasmasphere and radiation belt.
- The enhanced pressure inside the quasi-planar molded ICME could be the possible cause behind the observed significant compression of the magnetosphere.
- The case study suggests that the ICME transformed into a quasi-planar structure is causing the extreme storm.

- The statistical analysis of the geo-effectiveness of these planar structures is necessary to support the reported outcome. The statistical analysis will shortly be finished, and the results will be communicated very soon.

Acknowledgment We acknowledge use of NASA/GSFC's Space Physics Data Facility's OMNIWeb (or CDAWeb or ftp) service. We also thank the SOHO team for their remotely accessible data. This paper uses data from the Heliospheric Shock Database, generated and maintained at the University of Helsinki. We acknowledge SERB, India, since Anil Raghav is supported by SERB project reference file number CRG/2020/002314.

Author contributions AR proposed the project. ZS investigated the data in detail. AB, KG, OD, helped with the analysis. PV helps in the model analysis. AR, and ZS wrote the first draft after several discussions. AB, PV, and BD suggested corrections and improved the draft. Finally, all authors reviewed the manuscript.

Data Availability The utilized data in this analysis is taken from Wind spacecraft. The Wind data are publicly available at (1) NASA's Goddard Space Flight Center (GSFC) https://wind.nasa.gov/data.php, and (2) Coordinated Data Analysis Web (CDAWeb) https://cdaweb.gsfc.nasa.gov/pub/data/wind/.

Declarations

Competing interests The authors declare no competing interests.

References

Akasofu, S.-I.: 1981, Energy coupling between the solar wind and the magnetosphere. *Space Sci. Rev.* **28**(2), 121.

Akasofu, S.-I.: 2018, A review of the current understanding in the study of geomagnetic storms. *Int. J. Earth Sci. Geophys.* **4**(1), 18. DOI.

Baker, D., Kanekal, S., Li, X., Monk, S., Goldstein, J., Burch, J.: 2004, An extreme distortion of the Van Allen belt arising from the 'Hallowe'en' solar storm 2003. *Nature* **432**(7019), 878.

Balan, N., Skoug, R., Tulasi Ram, S., Rajesh, P., Shiokawa, K., Otsuka, Y., Batista, I., Ebihara, Y., Nakamura, T.: 2014, CME front and severe space weather. *J. Geophys. Res. Space Phys.* **119**(12), 10.

Balasis, G., Daglis, I., Zesta, E., Papadimitriou, C., Georgiou, M., Haagmans, R., Tsinganos, K.: 2012, ULF wave activity during the 2003 Halloween superstorm: multipoint observations from CHAMP, Cluster and Geotail missions. In: *Annales Geophysicae* **30**, 1751. DOI.

Bruinsma, S., Forbes, J.M., Nerem, R.S., Zhang, X.: 2006, Thermosphere density response to the 20–21 November 2003 solar and geomagnetic storm from Champ and Grace accelerometer data. *J. Geophys. Res. Space Phys.* **111(A6)**, A06303. DOI.

Burlaga, L., Sittler, E., Mariani, F., Schwenn, R.: 1981, Magnetic loop behind an interplanetary shock: Voyager, Helios, and IMP 8 observations. *J. Geophys. Res. Space Phys.* **86**(A8), 6673.

Cannon, P., Angling, M., Barclay, L., Curry, C., Dyer, C., Edwards, R., Greene, G., Hapgood, M., Horne, R.B., Jackson, D., et al.: 2013, *Extreme Space Weather: Impacts on Engineered Systems and Infrastructure*, Royal Academy of Engineering.

Chandra, R., Pariat, E., Schmieder, B., Mandrini, C.H., Uddin, W.: 2010, How can a negative magnetic helicity active region generate a positive helicity magnetic cloud? *Solar Phys.* **261**(1), 127. DOI. ADS

Chi, P., Russell, C., Foster, J., Moldwin, M., Engebretson, M., Mann, I.: 2005, Density enhancement in plasmasphere-ionosphere plasma during the 2003 Halloween superstorm: observations along the 330th magnetic meridian in North America. *Geophys. Res. Lett.* **32**(3), L03S07.

Chi, Y., Shen, C., Luo, B., Wang, Y., Xu, M.: 2018, Geoeffectiveness of stream interaction regions from 1995 to 2016. *Space Weather* **16**(12), 1960.

Cliver, E.W., Svalgaard, L.: 2004, The 1859 solar–terrestrial disturbance and the current limits of extreme space weather activity. *Solar Phys.* **224**(1 – 2), 407.

Daglis, I.A., Thorne, R.M., Baumjohann, W., Orsini, S.: 1999, The terrestrial ring current: origin, formation, and decay. *Rev. Geophys.* **37**(4), 407.

Davies, E.E., Möstl, C., Owens, M., Weiss, A., Amerstorfer, T., Hinterreiter, J., Bauer, M., Bailey, R., Reiss, M., Forsyth, R., et al.: 2021, In situ multi-spacecraft and remote imaging observations of the first CME detected by Solar Orbiter and BepiColombo. *Astron. Astrophys.* **656**, A2. DOI.

Desai, R.T., Zhang, H., Davies, E.E., Stawarz, J.E., Mico-Gomez, J., Iváñez-Ballesteros, P.: 2020, Three-dimensional simulations of solar wind preconditioning and the 23 July 2012 interplanetary coronal mass ejection. *Solar Phys.* **295**(9), 130.

Dungey, J.W.: 1961, Interplanetary magnetic field and the auroral zones. *Phys. Rev. Lett.* **6**(2), 47.

Eastwood, J., Biffis, E., Hapgood, M., Green, L., Bisi, M., Bentley, R., Wicks, R., McKinnell, L.-A., Gibbs, M., Burnett, C.: 2017, The economic impact of space weather: where do we stand? *Risk Anal.* **37**(2), 206.

Echer, E., Gonzalez, W., Tsurutani, B., Gonzalez, A.: 2008, Interplanetary conditions causing intense geomagnetic storms (Dst $\leq$ -100 nT) during solar cycle 23 (1996–2006). *J. Geophys. Res. Space Phys.* **113(A5)**, A05221. DOI.

Farrugia, C., Dunlop, M., Geurts, F., Balogh, A., Southwood, D., Bryant, D., Neugebauer, M., Etemadi, A.: 1990, An interplanetary planar magnetic structure oriented at a large (80 deg) angle to the Parker spiral. *Geophys. Res. Lett.* **17**(8), 1025.

Feng, X.: 2020, Current status of MHD simulations for space weather. In: *Magnetohydrodynamic Modeling of the Solar Corona and Heliosphere*, Springer, 1.

Fok, M.-C., Moore, T.E., Slinker, S.P., Fedder, J.A., Delcourt, D.C., Nosé, M., Chen, S.-H.: 2011, Modeling the superstorm in November 2003. *J. Geophys. Res. Space Phys.* **116**, A00J17. DOI.

Gold, T., Hoyle, F.: 1960, On the origin of solar flares. *Mon. Not. Roy. Astron. Soc.* **120**(2), 89.

Gonzalez, W., Mozer, F.: 1974, A quantitative model for the potential resulting from reconnection with an arbitrary interplanetary magnetic field. *J. Geophys. Res.* **79**(28), 4186.

Gonzalez, W., Joselyn, J.A., Kamide, Y., Kroehl, H.W., Rostoker, G., Tsurutani, B., Vasyliunas, V.: 1994, What is a geomagnetic storm? *J. Geophys. Res. Space Phys.* **99**(A4), 5771.

Gonzalez, W.D., Tsurutani, B.T.: 1987, Criteria of interplanetary parameters causing intense magnetic storms (Dst < 100 nT). *Planet. Space Sci.* **35**(9), 1101.

Gonzalez, W.D., Tsurutani, B.T., Gonzalez, A.L., Smith, E.J., Tang, F., Akasofu, S.-I.: 1989, Solar wind-magnetosphere coupling during intense magnetic storms (1978 – 1979). *J. Geophys. Res. Space Phys.* **94**(A7), 8835.

Gonzalez, W.D., De Gonzalez, A.C., Dal Lago, A., Tsurutani, B.T., Arballo, J.K., Lakhina, G., Buti, B., Ho, C.M., Wu, S.-T.: 1998, Magnetic cloud field intensities and solar wind velocities. *Geophys. Res. Lett.* **25**(7), 963.

Gopalswamy, N., Yashiro, S., Liu, Y., Michalek, G., Vourlidas, A., Kaiser, M., Howard, R.: 2005a, Coronal mass ejections and other extreme characteristics of the 2003 October–November solar eruptions. *J. Geophys. Res. Space Phys.* **110**, A09S15. DOI.

Gopalswamy, N., Yashiro, S., Michalek, G., Xie, H., Lepping, R., Howard, R.: 2005b, Solar source of the largest geomagnetic storm of cycle 23. *Geophys. Res. Lett.* **32**, L12S09. DOI.

Grechnev, V., Uralov, A., Chertok, I., Belov, A., Filippov, B., Slemzin, V., Jackson, B.: 2014b, A challenging solar eruptive event of 18 November 2003 and the causes of the 20 November geomagnetic superstorm. IV. Unusual magnetic cloud and overall scenario. *Solar Phys.* **289**(12), 4653.

Grechnev, V., Uralov, A., Slemzin, V., Chertok, I., Filippov, B., Rudenko, G., Temmer, M.: 2014a, A challenging solar eruptive event of 18 November 2003 and the causes of the 20 November geomagnetic superstorm. I. Unusual history of an eruptive filament. *Solar Phys.* **289**(1), 289.

Hapgood, M.: 2012, Astrophysics: prepare for the coming space weather storm. *Nature* **484**(7394), 311.

Hayakawa, H., Ebihara, Y., Pevtsov, A.A., Bhaskar, A., Karachik, N., Oliveira, D.M.: 2020, Intensity and time series of extreme solar-terrestrial storm in March 1946. *Mon. Not. Roy. Astron. Soc.* **497**(4), 5507.

Hu, Q., Sonnerup, B.U.: 2002, Reconstruction of magnetic clouds in the solar wind: orientations and configurations. *J. Geophys. Res. Space Phys.* **107**, 1142. DOI.

Jones, G., Balogh, A., Horbury, T.: 1999, Observations of heliospheric planar and offset-planar magnetic structures. *Geophys. Res. Lett.* **26**(1), 13.

Jones, G.H., Balogh, A.: 2001, Planar structuring of magnetic fields at solar minimum and maximum. *The 3-D Heliosphere at Solar Maximum* **97**, 165. DOI.

Kataoka, R., Watari, S., Shimada, N., Shimazu, H., Marubashi, K.: 2005a, Downstream structures of interplanetary fast shocks associated with coronal mass ejections. *Geophys. Res. Lett.* **32**, L12103. DOI.

Kataoka, R., Fairfield, D., Sibeck, D., Rastätter, L., Fok, M.-C., Nagatsuma, T., Ebihara, Y.: 2005b, Magnetosheath variations during the storm main phase on 20 November 2003: evidence for solar wind density control of energy transfer to the magnetosphere. *Geophys. Res. Lett.* **32**, L21108. DOI.

Kataoka, R., Ebisuzaki, T., Kusano, K., Shiota, D., Inoue, S., Yamamoto, T., Tokumaru, M.: 2009, Three-dimensional MHD modeling of the solar wind structures associated with 13 December 2006 coronal mass ejection. *J. Geophys. Res. Space Phys.* **114**, A10102. DOI.

Kataoka, R., Shiota, D., Kilpua, E., Keika, K.: 2015, Pileup accident hypothesis of magnetic storm on 17 March 2015. *Geophys. Res. Lett.* **42**(13), 5155.

Kilpua, E., Koskinen, H.E., Pulkkinen, T.I.: 2017, Coronal mass ejections and their sheath regions in interplanetary space. *Living Rev. Solar Phys.* **14**(1), 5.
Koehn, G.J., Desai, R.T., Davies, E.E., Forsyth, R.J., Eastwood, J.P., Poedts, S.: 2022, Successive interacting coronal mass ejections: how to create a perfect storm. *Astrophys. J.* **941**(2), 139.
Kumar, P., Manoharan, P., Uddin, W., Mahalakshmi, K.: 2011, On the source of the super-storm of solar-cycle# 23 associated with the solar flares on 18 November 2003. In: *Advances in Geosciences: Volume 27: Solar Terrestrial (ST)*, World Scientific, 129. DOI.
Kumar, S., Veenadhari, B., Tulasi Ram, S., Selvakumaran, R., Mukherjee, S., Singh, R., Kadam, B.: 2015, Estimation of interplanetary electric field conditions for historical geomagnetic storms. *J. Geophys. Res. Space Phys.* **120**(9), 7307.
Lakhina, G., Alex, S., Tsurutani, B., Gonzalez, W.: 2005, Research on historical records of geomagnetic storms. *Proc. Int. Astron. Union* **226**, 3. DOI.
Lepping, R., Behannon, K.: 1980, Magnetic field directional discontinuities: 1. Minimum variance errors. *J. Geophys. Res. Space Phys.* **85**(A9), 4695.
Liu, Y.D., Luhmann, J.G., Kajdič, P., Kilpua, E.K., Lugaz, N., Nitta, N.V., Möstl, C., Lavraud, B., Bale, S.D., Farrugia, C.J., et al.: 2014, Observations of an extreme storm in interplanetary space caused by successive coronal mass ejections. *Nat. Commun.* **5**, 3481.
Lugaz, N., Temmer, M., Wang, Y., Farrugia, C.J.: 2017, The interaction of successive coronal mass ejections: a review. *Solar Phys.* **292**(4), 64.
Lundquist, S.: 1950, Magnetohydrostatic fields. *Ark. Fys.* **2**, 361.
Manchester, W.B. IV, Gombosi, T.I., Roussev, I., De Zeeuw, D.L., Sokolov, I., Powell, K.G., Tóth, G., Opher, M.: 2004, Three-dimensional MHD simulation of a flux rope driven CME. *J. Geophys. Res. Space Phys.* **109**, A01102. DOI.
Mannucci, A., Tsurutani, B., Iijima, B., Komjathy, A., Saito, A., Gonzalez, W., Guarnieri, F., Kozyra, J., Skoug, R.: 2005, Dayside global ionospheric response to the major interplanetary events of October 29–30, 2003 "Halloween storms". *Geophys. Res. Lett.* **32**, L12S02. DOI.
Nakagawa, T.: 1993, Solar source of the interplanetary planar magnetic structures. *Solar Phys.* **147**(1), 169.
Nakagawa, T., Nishida, A., Saito, T.: 1989, Planar magnetic structures in the solar wind. *J. Geophys. Res. Space Phys.* **94**(A9), 11761.
Nakamizo, A., Tanaka, T., Kubo, Y., Kamei, S., Shimazu, H., Shinagawa, H.: 2009, Development of the 3-D MHD model of the solar corona-solar wind combining system. *J. Geophys. Res. Space Phys.* **114**(A7).
Neugebauer, M., Clay, D., Gosling, J.: 1993, The origins of planar magnetic structures in the solar wind. *J. Geophys. Res. Space Phys.* **98**(A6), 9383.
Ngwira, C.M., Pulkkinen, A., Leila Mays, M., Kuznetsova, M.M., Galvin, A., Simunac, K., Baker, D.N., Li, X., Zheng, Y., Glocer, A.: 2013, Simulation of the 23 July 2012 extreme space weather event: what if this extremely rare CME was Earth directed? *Space Weather* **11**(12), 671.
O'Brien, T., McPherron, R.: 2002, Seasonal and diurnal variation of Dst dynamics. *J. Geophys. Res. Space Phys.* **107**, 1341. DOI.
Odstrcil, D., Riley, P., Zhao, X.: 2004, Numerical simulation of the 12 May 1997 interplanetary CME event. *J. Geophys. Res. Space Phys.* **109**(A2).
Oliveira, D.M., Zesta, E., Hayakawa, H., Bhaskar, A.: 2020, Estimating satellite orbital drag during historical magnetic superstorms. *Space Weather* **18**, e02472. DOI.
Owens, M.J., Merkin, V., Riley, P.: 2006, A kinematically distorted flux rope model for magnetic clouds. *J. Geophys. Res. Space Phys.* **111**, A03104. DOI.
Palmerio, E., Kilpua, E.K., Savani, N.P.: 2016, Planar magnetic structures in coronal mass ejection-driven sheath regions. *Ann. Geophys.* **34**, 313.
Raghav, A., Bhaskar, A., Lotekar, A., Vichare, G., Yadav, V.: 2014, Quantitative understanding of Forbush decrease drivers based on shock-only and CME-only models using global signature of February 14, 1978 event. *J. Cosmol. Astropart. Phys.* **2014**, 074. DOI.
Raghav, A.N., Kule, A.: 2018a, Does the Alfvén wave disrupt the large-scale magnetic cloud structure? *Mon. Not. Roy. Astron. Soc.* **480**(1), L6.
Raghav, A.N., Kule, A.: 2018b, The first in situ observation of torsional Alfvén waves during the interaction of large-scale magnetic clouds. *Mon. Not. Roy. Astron. Soc. Lett.* **476**, L6. DOI.
Raghav, A.N., Shaikh, Z.I.: 2020, The pancaking of coronal mass ejections: an in situ attestation. *Mon. Not. Roy. Astron. Soc. Lett.* **493**(1), L16.
Riley, P., Crooker, N.: 2004, Kinematic treatment of coronal mass ejection evolution in the solar wind. *Astrophys. J.* **600**(2), 1035.
Riley, P., Linker, J., Mikić, Z.: 2001, An empirically-driven global MHD model of the solar corona and inner heliosphere. *J. Geophys. Res. Space Phys.* **106**(A8), 15889.
Savani, N., Owens, M., Rouillard, A., Forsyth, R., Kusano, K., Shiota, D., Kataoka, R., Jian, L., Bothmer, V.: 2011, Evolution of coronal mass ejection morphology with increasing heliocentric distance. II. In situ observations. *Astrophys. J.* **732**(2), 117.

Schrijver, C.J., Siscoe, G.L.: 2010, *Heliophysics: Space Storms and Radiation: Causes and Effects*, Cambridge University Press, Cambridge.

Shaikh, Z., Raghav, A., Bhaskar, A.: 2017, The presence of turbulent and ordered local structure within the ICME shock-sheath and its contribution to Forbush decrease. *Astrophys. J.* **844**(2), 121.

Shaikh, Z.I., Raghav, A., Vichare, G.: 2019, Coexistence of a planar magnetic structure and an Alfvén wave in the shock-sheath of an interplanetary coronal mass ejection. *Mon. Not. Roy. Astron. Soc.* **490**(2), 1638.

Shaikh, Z.I., Raghav, A.N.: 2022, Statistical plasma properties of the planar and nonplanar ICME magnetic clouds during solar cycles 23 and 24. *Astrophys. J.* **938**(2), 146.

Shaikh, Z.I., Raghav, A.N., Vichare, G., Bhaskar, A., Mishra, W.: 2018, The identification of a planar magnetic structure within the ICME shock sheath and its influence on galactic cosmic-ray flux. *Astrophys. J.* **866**(2), 118.

Shaikh, Z.I., Raghav, A., Vichare, G., Bhaskar, A., Mishra, W., Choraghe, K.: 2019, Concurrent effect of Alfvén waves and planar magnetic structure on geomagnetic storms. *Mon. Not. Roy. Astron. Soc.* **490**(3), 3440. DOI.

Shaikh, Z.I., Raghav, A.N., Vichare, G., Bhaskar, A., Mishra, W.: 2020, Comparative statistical study of characteristics of plasma in planar and non-planar ICME sheaths during solar cycles 23 and 24. *Mon. Not. Roy. Astron. Soc.* **494**(2), 2498.

Shiota, D., Kusano, K., Miyoshi, T., Shibata, K.: 2010, Magnetohydrodynamic modeling for a formation process of coronal mass ejections: interaction between an ejecting flux rope and an ambient field. *Astrophys. J.* **718**(2), 1305.

Shprits, Y., Thorne, R., Horne, R., Glauert, S., Cartwright, M., Russell, C., Baker, D., Kanekal, S.: 2006, Acceleration mechanism responsible for the formation of the new radiation belt during the 2003 Halloween solar storm. *Geophys. Res. Lett.* **33**, L05104. DOI.

Shue, J.-H., Song, P., Russell, C., Steinberg, J., Chao, J., Zastenker, G., Vaisberg, O., Kokubun, S., Singer, H., Detman, T., et al.: 1998, Magnetopause location under extreme solar wind conditions. *J. Geophys. Res. Space Phys.* **103**(A8), 17691.

Sonnerup, B.U., Scheible, M.: 1998, Minimum and maximum variance analysis. In: *Analysis Methods for Multi-Spacecraft Data*, 185.

Srivastava, N., Mathew, S.K., Louis, R.E., Wiegelmann, T.: 2009, Source region of the 18 November 2003 coronal mass ejection that led to the strongest magnetic storm of cycle 23. *J. Geophys. Res. Space Phys.* **114**, A03107. DOI.

Temerin, M., Li, X.: 2002, A new model for the prediction of Dst on the basis of the solar wind. *J. Geophys. Res. Space Phys.* **107**, 1472. DOI.

Tsurutani, B.T., Gonzalez, W.D.: 1997, The interplanetary causes of magnetic storms: a review. *Geophys. Monogr. Ser.* **98**, 77. DOI.

Tsurutani, B.T., Gonzalez, W.D., Tang, F., Akasofu, S.I., Smith, E.J.: 1988, Origin of interplanetary southward magnetic fields responsible for major magnetic storms near solar maximum (1978 – 1979). *J. Geophys. Res. Space Phys.* **93**(A8), 8519.

Tsurutani, B.T., Gonzalez, W.D., Tang, F., Lee, Y.T.: 1992, Great magnetic storms. *Geophys. Res. Lett.* **19**(1), 73.

Tsurutani, B.T., Gonzalez, W.D., Gonzalez, A.L., Guarnieri, F.L., Gopalswamy, N., Grande, M., Kamide, Y., Kasahara, Y., Lu, G., Mann, I., et al.: 2006, Corotating solar wind streams and recurrent geomagnetic activity: A review. *J. Geophys. Res. Space Phys.* **111**, A07S01. DOI.

Vemareddy, P., Möstl, C., Amerstorfer, T., Mishra, W., Farrugia, C., Leitner, M.: 2016, Comparison of magnetic properties in a magnetic cloud and its solar source on 2013 April 11 – 14. *Astrophys. J.* **828**(1), 12.

Welling, D.T., Love, J.J., Rigler, E.J., Oliveira, D.M., Komar, C.M., Morley, S.K.: 2021, Numerical simulations of the geospace response to the arrival of an idealized perfect interplanetary coronal mass ejection. *Space Weather* **19**, e02489. DOI.

Wu, C.-C., Liou, K., Hutting, L., Wood, B.E.: 2022, Magnetohydrodynamic simulation of multiple coronal mass ejections: an effect of "pre-events". *Astrophys. J.* **935**(2), 67.

Zhang, J., Liemohn, M.W., Kozyra, J.U., Thomsen, M.F., Elliott, H.A., Weygand, J.M.: 2006, A statistical comparison of solar wind sources of moderate and intense geomagnetic storms at solar minimum and maximum. *J. Geophys. Res. Space Phys.* **111**, A01104. DOI.

Zhang, J., Richardson, I., Webb, D., Gopalswamy, N., Huttunen, E., Kasper, J., Nitta, N., Poomvises, W., Thompson, B., Wu, C.-C., et al.: 2007, Solar and interplanetary sources of major geomagnetic storms (dst≤- 100 nt) during 1996–2005. *J. Geophys. Res. Space Phys.* **112**, A10102. DOI.

Zurbuchen, T.H., Richardson, I.G.: 2006, In-situ solar wind and magnetic field signatures of interplanetary coronal mass ejections. In: *Coronal Mass Ejections*, Springer, New York, 31.